HHS Public Access

Author manuscript

J Immunol. Author manuscript; available in PMC 2017 July 01.

Published in final edited form as:

J Immunol. 2016 July 1; 197(1): 288–295. doi:10.4049/jimmunol.1501946.

Defective association of the platelet glycoprotein Ib-IX complex with the glycosphingolipid-enriched membrane domain inhibits murine thrombus and atheroma formation

Hao Zhou[*,†,‡], **Yali Ran**[†,‡], **Qi Da**[†,‡], **Tanner S. Shaw**[†], **Dan Shang**[§,†], **Anilkumar K. Reddy**[†], **José A. López**[‖], **Christie M. Ballantyne**[†], **Jerry Ware**[#], **Huaizhu Wu**[†], and **Yuandong Peng**[†,¶]

[*]Department of Hospital Infection Management of Nanfang Hospital, Southern Medical University, China

[§]Department of Vascular Surgery, Union Hospital, Tongji Medical College, Huazhong University of Science and Technology, China

[‖]Puget Sound Blood Center, Division of Hematology, Department of Medicine, University of Washington, Seattle, Washington

[#]Departments of Physiology & Biophysics, University of Arkansas for Medical Sciences, Little Rock, Arkansas

[†]Cardiovascular Research Section, Department of Medicine, Baylor College of Medicine, Houston, Texas

Abstract

Localization of the platelet glycoprotein Ib-IX complex to the membrane lipid domain is essential for platelet adhesion to von Willebrand factor (vWf) and subsequent platelet activation *in vitro*. Yet, the *in vivo* importance of this localization has never been addressed. We recently found that the disulfide linkage between Ibα and Ibβ is critical for the association of Ibα with the glycosphingolipid-enriched membrane (GEM) domain, in this study, we established a transgenic mouse model expressing this mutant human Ibα that is also devoid of endogenous Ibα ($H\alpha_{SS}M\alpha^{-/-}$). Characterization of this model demonstrated a similar dissociation of Ibα from murine platelet GEMs to that expressed in CHO cells, which correlates well with the impaired adhesion of the transgenic platelets to vWf *ex vivo* and *in vivo*. Furthermore, we bred our transgenic mice into an atherosclerosis-prone background ($H\alpha_{SS}M\alpha^{-/-}ApoE^{-/-}$ and $H\alpha_{WT}M\alpha^{-/-}ApoE^{-/-}$). We observed that atheroma formation was significantly inhibited in mutant mice where fewer platelet-bound $CD11c^+$ leukocytes were circulating ($CD45^+/CD11c^+/CD41^+$) and residing in atherosclerotic lesions ($CD45^+/CD11c^+$), suggesting that platelet-mediated adhesion and infiltration of $CD11c^+$ leukocytes may be one of the mechanisms. These

[¶]Correspondence should be addressed to: Yuandong Peng, Cardiovascular Research Section, Department of Medicine, Baylor College of Medicine, One Baylor Plaza, Alkek N1317.06, Houston, Texas 77030. Tel: (713)798-8639; Fax: (713)798-3415; Yuandong@bcm.edu. .

[‡]These authors contributed equally to this paper

Disclosures

The authors have no financial conflicts of interest.

observations provide the first *in vivo* evidence showing that the membrane GEMs is physiologically and pathophysiologically critical in the function of the GP Ib-IX complex.

Introduction

The platelet glycoprotein (GP) Ib-IX complex is comprised of three type-I transmembrane proteins, GP Ibα, GP Ibβ and GP IX with a stoichiometry of 1:2:1, where two GP Ibβ (Cys122) molecules link with one GP Ibα (Cys484 and Cys485) through two extracellular membrane proximal disulfide bonds (1), and interact with GP IX in a non-covalent fashion (2,3). Lack of or dysfunction in GP Ib-IX causes Bernard-Soulier Syndrome (BSS) in humans, a bleeding disorder that is also recapitulated in several mouse models expressing no or mutant GP Ibα (4,5). It has been known that the GP Ib-IX-vWf interaction can be regulated by various mechanisms, the localization of the GP Ib-IX complex in reference to the cell membrane on either platelets or exogenous cell lines has recently been shown to play an important regulatory role (6-8). This special localization is conferred by the association of the GP Ib-IX complex with a specialized membrane domain enriched with glycosphingolipids, best known as GEMs (glycosphingolipid-enriched membranes) or raft. Lack of or dysfunction in this association caused by a disruption of platelet GEMs structure (e.g. MβCD treatment) (6) or introduction of a loss-of-association mutation to GP Ibα expressed in Chinese Hamster Ovary (CHO) cells (7) eliminates or inhibits the function of the GP Ib-IX complex, in particular, the high shear-induced vWf binding of and signal transmission by the GP Ib-IX complex. Nevertheless, the physiological or pathophysiological relevance of the GEMs in the function of the GP Ib-IX complex has never been addressed and established.

We recently demonstrated that disrupting the α/β disulfide linkage decreased the GP Ibα-GEMs association level in CHO cells resulting in a marked inhibition of vWf binding at high shear (7). In this study, we expressed this GEMs-association dysfunctional GP Ibα in mice, and employed a ferric chloride induced thrombosis and a high cholesterol diet induced atherosclerosis model to investigate the physiological and pathophysiological roles of the GEMs in the function of the GP Ib-IX complex.

Methods

Mice and diets

The transgenic mouse expressing the disulfide linkage deficient human GP Ibα was generated in the Transgenic and Stem Cells Core Facility at the University of Texas Health Science Center-Houston. The mice used in our thrombosis and atherosclerosis models were age and gender matched littermates. In brief, we injected a 6~kb *EcoR*I fragment possessing the entire cassette for human GP Ibα expression in mice (9) into mouse zygotes (C57BL/6J strain) and implanted pseudopregnant females with the fertilized embryos. After birth, we performed a polymerase chain reaction (PCR) based approach to screen the offspring for the human GP Ibα gene in the genome. Further breeding of these positive mice to the wild-type animals demonstrated that 5 out of the 12 mice in the F1 generation stably carried the human GP Ibα gene and 3 expressed the human GP Ibα mRNA. We then crossed these 3 mice with

the GP Ibα deficient animals ($M\alpha^{-/-}$) to remove the coding sequence for the mouse GP Ibα polypeptide. One resulting line was chosen ($H\alpha_{SS}M\alpha^{-/-}$) because of its lack of endogenous murine GP Ibα and expression of human GP Ibα on the platelets surface in a level comparable to that in the wild-type GP Ibα-expressing transgenic murine platelets ($H\alpha_{WT}M\alpha^{-/-}$) (10). In our atherosclerosis study, we took a two-step approach to breed our transgenic mice to an atherosclerosis-prone background. First, we crossed the murine GP Ibα deficient mice ($M\alpha^{-/-}$) with ApoE knockout mice ($ApoE^{-/-}$) to obtain mice that lack both murine GP Ibα and ApoE ($M\alpha^{-/-}ApoE^{-/-}$); second, we crossed these $ApoE^{-/-}M\alpha^{-/-}$ mice with the human GP Ibα-expressing transgenic mice ($H\alpha_{WT}M\alpha^{-/-}$ and $H\alpha_{SS}M\alpha^{-/-}$), respectively, to obtain two novel atherosclerosis-prone mouse lines ($H\alpha_{WT}/M\alpha^{-/-}ApoE^{-/-}$ and $H\alpha_{SS}/M\alpha^{-/-}ApoE^{-/-}$). The deficiency of the murine $ApoE^{-/-}$, murine GP Ibα ($M\alpha^{-/-}$), and the appearance of the human GP Ibα mRNA (Hα) was verified either by a polymerase chain reaction (PCR) with specific primers for murine ApoE and human GP Ibα or by flow cytometry analysis of the surface expression of both human and mouse GP Ibα. Mice were fed a normal diet (ND) or a high cholesterol diet (HCD; 21% fat [w/w], 0.15% cholesterol [w/w], Dyet 112734, Dyets Inc.) beginning at the age of 6 months and maintained on a HCD for 16 weeks. All animal experiments were done upon an approval from the Institutional Animal Care and Use Committee (IACUC) of Baylor College of Medicine or National Institutes of Health Office of Laboratory Animal Welfare.

Sucrose density gradient centrifugation

Resting murine platelets were lysed with 1.6 ml ice-cold Brij 35 MES-buffered saline (MBS) [25 mM MES, pH 6.5, 150 mM NaCl, 2 × proteinase inhibitor (Roche Diagnostics)] on ice for 1 hr (7). The sample was then mixed with 1.6 ml of 80% sucrose in MES, transferred to the bottom of a 14×95 mm centrifuge tube (Seton Scientific) and gently overlaid with 4.8 ml 30% and then 1.6 ml 5% sucrose in MES. The gradient was then centrifuged at 34,000 rpm (~146,000 × g) in a SW40.Ti rotor (Beckman) for 18 h at 4°C followed by fractionation (from the top of the gradient) into twelve 800 μl samples. Equal volumes (15 μl) of each fraction were resolved using an SDS-PAGE gel, and transferred to a PVDF membrane. GP Ibα was detected by western blotting. The GEMs fractions were identified by the presence of flotillin, a known GEM-specific marker.

Flow chamber assay

Sodium citrate anticoagulated murine whole blood was perfused over human immobilized vWf (10 μg/ml) in a parallel-plate flow chamber at shear rates of either $1{,}500s^{-1}$ or $15{,}000s^{-1}$. The experiments were recorded in real time by a high-speed digital camera (Model Quantix; Photometrics, Tucson, AZ) connected to an inverted-stage microscope (Eclipse TE300; Nikon, Garden City, NY).

Ristocetin-induced vWf binding to transgenic murine platelets

Murine whole blood was collected from the inferior vena cava and mixed with acid-citrate dextrose solution (85 mM trisodium citrate, 71 mM citric acid, and 111mM dextrose) in a 6:1 ratio. After diluting it with an equal volume of 1× DPBS (Invitrogen), the blood was centrifuged at 90×*g* for 20 min and the platelet-rich plasma (PRP) was collected and centrifuged at 750×*g* for 10 min in the presence of 50ng/ml prostacyclin. The pelleted

platelets were then suspended and washed twice with 1×PBS in the presence of 50ng/ml prostacyclin. After the final wash, platelets were resuspended in 1×PBS buffer to a concentration of 2.0×10^8/ml. The aggregometry analyses of vWf binding to either wild type or mutant platelets (2×10^5/ml) under stirring conditions were performed in the presence of 1.5mg/ml ristocetin (Sigma) and 10μg/ml human vWf (Sekisui Diagnostics) with an eight channel Bio/Data PAP-8C aggregometer (Biodata Corporation).

Platelet spreading on immobilized vWf

One hundred microliter of washed murine platelets (2×10^8/ml) were gently mixed with 1.5mg/ml ristocetin and incubated on immobilized human vWf (10μg/ml) in the presence of 0.8 mM Ca^{2+}/1.2mM Mg^{2+} for 1, 2, and 3 hours at 37ºC. After washing, the adherent platelets were fixed with 4% paraformaldhyde for 15 min at room temperature and stained with a rhodamine-labeled phalloidin (11) to reveal the morphological changes i.e., filopodia and lamellipodia. The spreading was imaged with a Nikon E800 fluorescence microscope. Each spreading experiment was performed at least 3 times and at least 10 fields of view were counted to calculate the average number of adherent platelets.

Ferric chloride thrombosis model and tail bleeding time

The right common carotid artery of an anesthetized (1.5% isofluorane) murine mouse at age 6 month was exposed to a 10×10 mm strip of 3MM Waterman filter paper saturated in a 10% $FeCl_3$ solution for 3 min. After rinsing three times with phosphate-buffered saline, the blood flow and ECG signal were monitored using a PC-based high-speed real-time Doppler signal processing system (12-15). The occlusion time was counted as the period from removal of the filter paper to the time when the Doppler signal went to nearly zero. Mouse tail bleeding times were determined by removing 3 mm of distal tail tissue and immediately immersing the tail into 37°C 1×PBS. The time from incision to cessation of blood was defined as the tail bleeding time.

Oil red staining and quantification of atherosclerotic lesions in whole aortas

After 16 weeks on HCD, complete mouse aortas were isolated from the ascending aorta to the iliac bifurcation, and then stained with oil red as previously described (16). In brief, mouse aortas were cut open and pinned on a blue wax tissue processing disc (Braintree Scientific Inc). After quickly rinsing with ddH_2O and then 70% isopropanol, a ~1.8% solution (w/v) of oil red (Sigma) in a solvent mixture of isopropanol:water (3:2) was added and incubated with the tissues for 30 min. After staining, the aortas were washed with 70% isopropanol followed by ddH_2O. Digital images of the stained aortas were captured using a dissection microscope attached to a Canon camera, and surface area of the atherosclerotic lesions were quantified using Image J software (17,18).

Antibody and flow cytometry analysis of circulating leukocyte-platelet aggregates (19)

Two hundred microliters of facial blood were obtained from a mouse and mixed with 20μl of 3.8% sodium citrate. The blood/sodium citrate mixture was then fixed in 1% paraformaldehyde (PFA) at room temperature for 10 min. Following fixation 8 ml of red blood cell lysing buffer (Sigma) were added and incubated on ice for 10 min. After

incubation, 1 ml of 10× DPBS (Invitrogen) was added and mixed thoroughly then centrifuged at 1,800×*g* for 2 min. The pellet was then resuspended in 1× DPBS. The white blood cells were then blocked with rat whole IgG (Jackson ImmunoResearch) and hamster whole IgG (Biolegend) at 4ºC for 5 min. After blocking the following antibodies were used to identify interactions: PE/Cy5-CD45 (Biolegend), PE-CD11c (Biolegend), FITC-CD41 (BD Biosciences). For controls the following isotype-matched antibodies were used: PE/Cy5-Rat IgG_{2b} (Biolegend), PE-Hamster $IgG_{1\kappa}$ (Biolegend) and FITC-Rat IgG_1 (Biolegend). The mixtures of antibodies and white blood cells were then incubated on a rotator for 30 min at room temperature and then measured with a Coulter Epics XL-MCL Flow Cytometer and analyzedCoulter Epics XL-MCL) Coulter Epics XL-MCL) using EXPO32 ADC software (Beckman Coulter).

Flow cytometry analysis for the infiltration of leukocytes into mouse aorta

Mice were sacrificed after feeding HCD for 4 months and cleared of blood by flushing the system with 30 ml of 1× DPBS. The aorta was then dissected out and cut into 1-2 mm pieces and digested with a mixture of 125U/ml Collagenase XI (Sigma), 450 U/ml Collagenase type 1 (Sigma), 60 U/ml Hyaluronidase type 1 (Sigma), and 60 U/ml DNase I (Roche) in a DPBS/20mM Hepes buffer, pH7.2 (19). The tube was mixed and placed into a 42ºC water bath for 1 hour and mixed every 10 min. Following digestion, the mixture was passed through a 70 μm cell strainer (Falcon), and then centrifuged at 850×*g* for 2 min. After centrifugation the cells were fixed in 1% PFA for 10 min at room temperature, washed, and resuspended with 1× DPBS. The cells were then incubated with the same blocking agents, antibodies, and isotype control antibodies for 30min at room temperature prior to flow cytometry analysis. The same antibodies and procedures in the leukocyte/platelet aggregation assay were used to identify CD45, CD11c and CD41.

Statistical Analysis

SPSS 21.0 was used for statistical analyses. Values are presented as mean±SEM. Student t tests (for comparison between 2 groups) or one-way ANOVA (for comparisons of ≥3 groups) with Newman-Keuls multiple comparison or nonparametric tests were used for statistical analyses. *Indicates a p-value <0.05, ***indicates a p-value <0.01.

Results

The physiological role of the GEMs in the function of the GP Ib-IX complex

Because platelets are anucleate, it is not possible to manipulate platelet gene structure and expression by employing traditional approaches. We therefore went on to generate transgenic mice expressing the GEMs-association-dysfunctional human GP Ibα ($Hα_{SS}$) (7). As shown in Fig. 1A, both wild type and mutant human GP Ibα express on the murine platelets with comparable levels, also no endogenous murine GP Ibα was detected as shown by a FITC-labeled rat anti-mouse GP Ibα specific antibody. Of note, a comparable level of mutant human GP Ibα can only be achieved and maintained after the mice have reached the age of 4 months. Even though we do not know the underlying mechanism for the delayed expression, consistent with our previous observations in CHO cells (7), we observed significantly less percentage of the mutant transgenic GP Ibα that localizes to the platelet

GEMs when compared to the wild type transgenic GP Ibα (Fig. 1B and 1C, 33±1.8% *vs* 50±4.2%). Furthermore, this reduction does not affect the static binding of human vWf to the transgenic platelets induced by ristocetin, a modulator that can only promote bond formation between human GP Ibα and vWf (Fig. 2A). In contrast, both the interaction of GP Ibα with immobilized vWf at high shear (Fig. 2B), and $\alpha_{IIb}\beta_3$-mediated platelet morphological changes (Fig. 2C) were attenuated upon the removal of the α/β disulfide linkage. In the former, we observed that the mutant platelets rolled at a velocity ~2 times faster than the wild type when perfused at a shear rate of 15,000s^{-1}. However, at a shear rate of 1,500s^{-1} the difference was much less prominent, indicating that the changes in the multivalency of the GP Ibα-vWf bond due to α/β disulfide linkage deficiency cannot be revealed until high shear force is imposed. To the latter, we found that upon adhesion to immobilized vWf, both transgenic platelets were able to undergo a morphological change, progressively switching from filopodia protrusion to lamellipodia spreading (Fig. 2C, left panel). However, compared to the wild type where more than 80% of the platelets fully spread (lamellipodia) within 3 hours, approximately only 60% of mutant platelets did so, indicative of a much slower $\alpha_{IIb}\beta_3$ activation in the mutant platelets (Fig. 2C, right panel).

To further address the physiological relevance of these *ex vivo* findings, we went on to examine the transgenic mice in a ferric chloride-induced thrombosis model (Fig. 3), a common model used in the research of the GP Ib-IX complex (20-23). We treated mouse carotid arteries with 10% $FeCl_3$ (Fig. 3A, upper panel) and monitored the blood flow with a Doppler system (Fig.3A, lower panel) (12-15). We found that the mice expressing wild type GP Ibα occluded their vessels faster than the mutant mice, where the blood flow in 2 out of 14 mutant mice did not even stop (Fig. 3B, open circle). Importantly, we never observe the reperfusion of blood flow in either mouse line 30 min after first occlusion, suggesting that the dysfunction in the GP Ib-IX-GEMs association did not abolish the GP Ibα function, instead, only inhibited it. In agreement, we found that the tail bleeding times were comparable between these two transgenic mouse lines, demonstrating that under low shear stresses mutations we introduced to the GP Ibα does not significantly impact the vWf/GP Ibα-mediated hemostasis in both mice (Fig. 3C). Taken together, by comparing the two transgenic platelets in several *ex vivo* and *in vivo* assays, we demonstrated that the disulfide linkage deficiency inhibits GP Ibα localization to platelet GEMs leading to an impairment of the GP Ibα function, in particular, high shear induced vWf binding and $\alpha_{IIb}\beta_3$ activation.

The pathophysiological role of the GEMs in the function of the GP Ib-IX complex

Several lines of investigation have suggested that vWf participates in atherogenesis through mediating platelet adhesion to atherosclerotic lesions (24-26). Compared to an acute release (within minutes) of vWf induced by vascular injury, e.g., $FeCl_3$ treatment, atherogen stimulates endothelial cells to release vWf chronically (from weeks to months). Because of the evident impairment of vWf binding and the signal transmitting function of the GP Ib-IX complex in our mutant transgenic mice, we postulated such dysfunction may compromise atheroma formation due to an inhibition of the vWf-GP Ib-IX interaction. We bred our transgenic and GP Ibα deficient mice to an atherosclerosis-prone background ($ApoE^{-/-}$) and fed them a high cholesterol diet (HCD) starting at the age of 6 months. After 16-week on HCD, the wild type human GP Ibα transgenic mice developed extensive atherosclerotic

lesions. In contrast, the GP Ibα mutant and deficient ApoE mice developed apparent but significantly fewer severe atherosclerotic lesions in their aortas, as revealed by oil red staining (Fig. 4A). Quantification of the lesion areas in these mice showed a clear and quantifiable amount of variation in severity (Fig. 4B). In addition, we also included the $ApoE^{-/-}$ only mice in our experiment as a control, and found that these mice formed atherosclerotic lesions with comparable sizes to the transgenic $ApoE^{-/-}$ mice expressing wild type human GP Ibα. This result suggests that the genetic manipulation of GP Ibα has a minor effect, if any, on the severity of the lesions we observed in this study. By preparing single cell suspensions from these atherosclerotic aortas and labeling them with a PE-Cy5-labeled antibody against CD45, a general leukocyte marker, we found that the number of infiltrated $CD45^+$ leukocytes in atherosclerotic vessels was progressively reduced, with the most being found in GP Ibα-wild type, fewer in the mutated version, and the lowest being found in GP Ibα-knockout mice (Fig. 4C). These data correlated well with the variation of the lesion sizes in these animals, indicating that the alleviated atheroma formation resulted specifically from a dysfunction or a loss of function in the GP Ib-IX complex. Consistent with our previous finding on the critical role of $CD11c^+$ cells in atherogenesis (27), we found that there was a significantly reduced portion of $CD11c^+$ cells in the lesions of mutant and GP Ibα deficient mice than in the wild type animals (Fig. 4D). Interestingly, the infiltrated $CD11c^+$ cells were reduced to a greater extent than other $CD45^+$ cell types in mutant and GP Ibα deficient mice relative to the wild type animals (Fig. 4E), indicating that platelets may preferentially facilitate these $CD11c^+$ cells to infiltrate into atherosclerotic lesions and contribute to the development of atherosclerosis.

It has been reported that in patients platelet reactivity and circulating leukocyte-platelet aggregates are increased with coronary artery diseases (28-31). In animals, platelet-leukocyte interactions have also been found to be critical for the initiation and progression of atherosclerosis. For instance, in hypercholesterolemic animals (with a similar experimental setting as ours), the endothelium is deposited with platelet-leukocyte aggregates which makes it more prone to plaque formation (32). Because we previously demonstrated that the $CD11c^+$ monocytes play a critical role in atherogenesis in $ApoE^{-/-}$ mice fed HCD, here we examined if platelets may bind to these cells to promote their atherogenic function. To achieve this, we first stained the pooled whole blood samples with the same PE-Cy5-labeled anti-CD45 antibody and then analyze the CD45-gated CD11c and CD41 triple positive cells (leukocyte-platelet aggregates) (Fig. 5A). We found that the wild type atherosclerotic mice have a significantly higher number of $CD45^+CD41^+$ cells when compared to the mutant mice (Fig. 5B). To our surprise, as shown in Fig. 5A, we found that nearly all (>98%) of these platelet-bound leukocytes are also CD11c positive ($CD45^+CD41^+CD11c^+$). Interestingly, in circulation, there appears to be an accumulation of the free $CD11c^+$ cells in the knockout mice when compared to wild type and mutant animals (Fig. 5C). This suggests that in the absence of platelets infiltration of $CD11c^+$ leukocytes is greatly attenuated, leading to a significant decrease in atherosclerosis in these mice. Furthermore, we have previously reported that >85% of these $CD11c^+$ cells in the circulation of this mouse model are lipid-laden foamy monocytes rather than lymphocytes and neutrophils, which do not express CD11c (27,33,34). They infiltrate into the atherosclerotic vessel walls and are selectively localized in atherosclerotic lesions (27,34,35). Our results suggest that GP Ibα-

harboring platelets are important in facilitating the adhesion and infiltration of these CD11c positive monocytes during atheroma formation.

Discussion

It is well known that the interaction between GP Ib-IX and vWf captures flowing platelets, initiates the slow translocation of platelets (36,37), and activates platelet integrins (e.g. $\alpha_{IIb}\beta_3$ and $\alpha_2\beta_1$) leading to firm arrest of the tethered platelets (36-40). Current belief is that the GP Ib-IX complex needs to be present in the platelet membrane GEMs domain in order to provide sufficient avidity for the GP Ibα-vWf bond strength as well as act as a platform for the assembly of downstream signaling molecules to activate platelet integrins. Although the first observations on the role of GEMs in GP Ib-IX function were made from an *in vitro* experiment more than 10 years ago, the physiological or pathophysiological relevance of the GEMs in the function of this complex have never been addressed. We recently observed that disrupting the α/β disulfide linkage markedly decreased the amount of GP Ibα instead of β/IX that is associated with the GEMs in CHO cells, and this partial dissociation inhibited the function of the GP Ib-IX complex in vWf binding at high shear (7). In this study, we report a novel transgenic mouse model expressing α/β disulfide linkage deficient GP Ibα. This mutant GP Ibα is also dysfunctional in the localization to the murine platelet GEMs domain which caused several apparent inhibitory effects including impaired shear-induced platelet tethering to surface-bound vWf at high shear, significantly delayed morphological changes of the cells, and a longer vessel occlusion time upon $FeCl_3$-induced vascular injury *in vivo*. On the other hand, we did notice that the difference between these two mice in their shear-induced vWf binding can only be revealed at a shear rate of 15,000s^{-1}, a condition that is generally not seen *in vivo*, suggesting that the major impact upon α/β disulfide linkage deficiency was on the GP Ib-IX-vWf binding induced $\alpha_{IIb}\beta_3$ activation. Further investigations are needed in order to identify the structural necessity of the β/IX complex to achieve a better inhibition or even an elimination of the GP Ib-IX-GEMs association where both the shear-induced binding function and the vWf-binding induced signaling function of the GP Ib-IX complex could be simultaneously abolished *in vivo* (7,41).

In order to investigate if a dysfunction in the GEMs association affects the GP Ib-IX complex-mediated platelet adhesion in a GP Ib-IX-related disease setting (25,42), we bred our transgenic mouse model with an atherosclerosis-prone mouse. In comparison to the wild type animals, we found that atheroma formation was attenuated in the mutant animals after feeding them a HCD for 4 months where the number of infiltrated leukocytes in atherosclerotic vessels is reduced in mutant and knockout mice, indicating that our findings were specific to the role of the GP Ib-IX complex in atherogenesis. Interestingly, because we also found a similar decrease in the percentage of the platelet-leukocyte aggregates in circulation, our data suggest that the attenuation was imposed even prior to the infiltration of inflammatory cells into atherogen-stimulated vessel walls.

Based on previous investigations and the data generated from our thrombosis and atherosclerosis models in this study, it is possible that the alleviation of atherosclerosis upon GP Ibα dysfunction results from a combined impairment of GP Ibα-mediated interactions (Fig. 6), including 1) impaired interaction between GP Ibα with vWf causing inefficient

spreading of adherent platelets (Interaction I) and fewer platelet-bound leukocytes to adhere to the atherosclerotic vessel walls (Interaction III), and 2) impaired interaction between GP Ibα and its ligands on the leukocytes surface (e.g. CD11b, Interaction II) causes fewer platelets to interact with leukocytes. Because the shear force on the vWf-GP Ibα bond will be largely increased when the platelets are pre-bound by leukocytes (1,2), the mutant GP Ibα-vWf bonds are weaker when compared to the wild type in supporting constant contact between platelet-bound leukocytes and the atherosclerotic vessels, which causes a decrease in the number of leukocytes that are captured onto the vessel walls and infiltrated into the atherosclerotic lesions in the mutant animals (Interaction III). In circulation, we observed that the platelet-leukocyte aggregate counts ($CD45^+CD41^+$) are decreased by ~40% in the mutant animals relative to the wild type animals (Fig. 5B), and nearly all these $CD45^+CD41^+$ aggregates are also CD11c positive (Fig. 5A), demonstrating that fewer numbers of $CD11c^+$ cells are bound by the mutant platelets than the wild type platelets (the counts of the circulating $CD11c^+$ cells are comparable between these two animals (Fig.5C)). Thus, our results suggest that the binding of the platelets to the $CD11c^+$ cells is impaired in the mutant animals, which is possibly due to an inhibition of the interaction between GP Ibα and its ligands on the $CD11c^+$ cells (e.g. CD11b) upon GP Ibα mutation (Interaction II). Because lack of the α/β disulfide linkage in the GP Ib-IX complex impairs the spreading of the transgenic platelets on an immobilized vWf surface (Fig 2C), one would expect that wild type platelets, once adhere to the vWf-bound atherosclerotic vessel walls (Interaction I), will spread better than the mutant platelets and provide a better surface to recruit and facilitate more inflammatory leukocytes to infiltrate into atherosclerotic lesions through an interaction between GP Ibα and its ligands on the leukocyte cells (Interaction II). Our data suggest that GP Ibα plays a critical role in the recruitment and infiltration of $CD11c^+$ monocytes to the atherosclerotic vessel wall, a process that is inhibited by dysfunction in or lack of GP Ibα, thus alleviating atherosclerosis in the mutant and knockout animals. Although the mechanism through which this impairment functions to prohibit atherosclerosis will continue to be investigated in future studies, these data demonstrate a novel role of GP Ibα in facilitating the adhesion and infiltration of the $CD11c^+$ monocytes.

Taken together, our study shows that interference in the function of the GP Ib-IX complex by inhibition of GP Ibα localization to the GEM domain cannot only prolong thrombotic vessel occlusion upon vascular injury but also inhibit inflammatory atherosclerosis, two settings that we used in this study to address the physiological and pathophysiological relevance of the GEMs domain in the function of the GP Ib-IX complex. In addition, because the mutations we introduced into GP Ibα are confined to a region that does not participate in the bindings of any identified GP Ib-IX ligands, we believe that our newly generated transgenic mouse expressing a GEMs-association dysfunctional GP Ibα is a unique model that allows a detailed mechanistic investigation into the specific roles of either the GEMs in the function of the GP Ib-IX complex or the GP Ib-IX complex in various physiological and pathological processes.

Acknowledgements

None

This work was supported by the American Heart Association (Scientist Development Grant 0635155N) (Y.P.), the National Institutes of Health (grant HL095676) (Y.P.) and (grant HL098839) (H.W.), Alkek Endowment Fund (Y.P.) and the Fondren Foundation (Y.P.).

Abbreviations used in this article

GP Ib-IX	glycoprotein Ib-IX
vWf	von Willebrand factor
GEMs	glycosphingolipid-enriched membranes
BSS	Bernard-Soulier syndrome
HCD	high cholesterol diet

References

1. Luo SZ, Mo X, fshar-Kharghan V, Srinivasan S, Lopez JA, Li R. Glycoprotein Ibalpha forms disulfide bonds with 2 glycoprotein Ibbeta subunits in the resting platelet. Blood. 2007; 109:603–609. [PubMed: 17008541]
2. Berndt MC, Gregory C, Kabral A, Zola H, Fournier D, Castaldi PA. Purification and preliminary characterization of the glycoprotein Ib complex in the human platelet membrane. Eur. J. Biochem. 1985; 151:637–649. [PubMed: 3161731]
3. Mo X, Nguyen NX, McEwan PA, Zheng X, Lopez JA, Emsley J, Li R. Binding of platelet glycoprotein Ibbeta through the convex surface of leucine-rich repeats domain of glycoprotein IX. J. Thromb. Haemost. 2009; 7:1533–1540. [PubMed: 19566547]
4. López JA, Andrews RK, Afshar-Kharghan V, Berndt MC. Bernard-Soulier Syndrome. Blood. 1998; 91:4397–4418. [PubMed: 9616133]
5. Bergmeier W, Chauhan AK, Wagner DD. Glycoprotein Ibalpha and von Willebrand factor in primary platelet adhesion and thrombus formation: lessons from mutant mice. Thromb. Haemost. 2008; 99:264–270. [PubMed: 18278173]
6. Shrimpton CN, Borthakur G, Larrucea S, Cruz MA, Dong JF, Lopez JA. Localization of the adhesion receptor glycoprotein Ib-IX-V complex to lipid rafts is required for platelet adhesion and activation. J. Exp. Med. 2002; 196:1057–1066. [PubMed: 12391017]
7. Geng H, Xu G, Ran Y, Lopez JA, Peng Y. Platelet glycoprotein Ib beta/IX mediates glycoprotein Ib alpha localization to membrane lipid domain critical for von Willebrand factor interaction at high shear. J. Biol. Chem. 2011; 286:21315–21323. [PubMed: 21507943]
8. Jin W, Inoue O, Tamura N, Suzuki-Inoue K, Satoh K, Berndt MC, Handa M, Goto S, Ozaki Y. A role for glycosphingolipid-enriched microdomains in platelet glycoprotein Ib-mediated platelet activation. J. Thromb. Haemost. 2007; 5:1034–1040. [PubMed: 17461932]
9. Ware J, Russell SR, Marchese P, Ruggeri ZM. Expression of human platelet Glycoprotein Ibα in transgenic mice. J. Biol. Chem. 1993; 268:8376–8382. [PubMed: 8463345]
10. Ware J, Russell S, Ruggeri ZM. Generation and rescue of a murine model of platelet dysfunction: the Bernard-Soulier syndrome. Proc. Natl. Acad. Sci. U. S. A. 2000; 97:2803–2808. [PubMed: 10706630]
11. Gu M, Xi X, Englund GD, Berndt MC, Du X. Analysis of the roles of 14-3-3 in the platelet glycoprotein Ib-IX- mediated activation of integrin $\alpha_{IIb}\beta_3$ using a reconstituted mammalian cell expression model. J. Cell Biol. 1999; 147:1085–1096. [PubMed: 10579727]
12. Hartley CJ, Reddy AK, Madala S, Martin-McNulty B, Vergona R, Sullivan ME, Halks-Miller M, Taffet GE, Michael LH, Entman ML, Wang YX. Hemodynamic changes in apolipoprotein E-knockout mice. Am. J. Physiol Heart Circ. Physiol. 2000; 279:H2326–H2334. [PubMed: 11045969]

13. Li YH, Reddy AK, Taffet GE, Michael LH, Entman ML, Hartley CJ. Doppler evaluation of peripheral vascular adaptations to transverse aortic banding in mice. Ultrasound Med. Biol. 2003; 29:1281–1289. [PubMed: 14553805]
14. Reddy AK, Taffet GE, Li YH, Lim SW, Pham TT, Pocius JS, Entman ML, Michael LH, Hartley CJ. Pulsed Doppler signal processing for use in mice: applications. IEEE Trans. Biomed. Eng. 2005; 52:1771–1783. [PubMed: 16235663]
15. Reddy AK, Madala S, Jones AD, Caro WA, Eberth JF, Pham TT, Taffet GE, Hartley CJ. Multichannel pulsed Doppler signal processing for vascular measurements in mice. Ultrasound Med. Biol. 2009; 35:2042–2054. [PubMed: 19854566]
16. Beattie JH, Duthie SJ, Kwun IS, Ha TY, Gordon MJ. Rapid quantification of aortic lesions in apoE(−/−) mice. J. Vasc. Res. 2009; 46:347–352. [PubMed: 19142014]
17. Nicoletti A, Kaveri S, Caligiuri G, Bariety J, Hansson GK. Immunoglobulin treatment reduces atherosclerosis in apo E knockout mice. J. Clin. Invest. 1998; 102:910–918. [PubMed: 9727059]
18. Johansson ME, Zhang XY, Edfeldt K, Lundberg AM, Levin MC, Boren J, Li W, Yuan XM, Folkersen L, Eriksson P, Hedin U, Low H, Sviridov D, Rios FJ, Hansson GK, Yan ZQ. Innate immune receptor NOD2 promotes vascular inflammation and formation of lipid-rich necrotic cores in hypercholesterolemic mice. Eur. J. Immunol. 2014; 44:3081–3092. [PubMed: 25042478]
19. Galkina E, Kadl A, Sanders J, Varughese D, Sarembock IJ, Ley K. Lymphocyte recruitment into the aortic wall before and during development of atherosclerosis is partially L-selectin dependent. J. Exp. Med. 2006; 203:1273–1282. [PubMed: 16682495]
20. Liu J, Fitzgerald ME, Berndt MC, Jackson CW, Gartner TK. Bruton tyrosine kinase is essential for botrocetin/VWF-induced signaling and GPIb-dependent thrombus formation in vivo. Blood. 2006; 108:2596–2603. [PubMed: 16788103]
21. Bergmeier W, Piffath CL, Goerge T, Cifuni SM, Ruggeri ZM, Ware J, Wagner DD. The role of platelet adhesion receptor GPIbalpha far exceeds that of its main ligand, von Willebrand factor, in arterial thrombosis. Proc. Natl. Acad. Sci. U. S. A. 2006; 103:16900–16905. [PubMed: 17075060]
22. Guerrero JA, Shafirstein G, Russell S, Varughese KI, Kanaji T, Liu J, Gartner TK, Baumler W, Jarvis GE, Ware J. In vivo relevance for platelet glycoprotein Ibalpha residue Tyr276 in thrombus formation. J. Thromb. Haemost. 2008; 6:684–691. [PubMed: 18339097]
23. Joglekar MV, Ware J, Xu J, Fitzgerald ME, Gartner TK. Platelets, glycoprotein Ib-IX, and von Willebrand factor are required for FeCl(3)-induced occlusive thrombus formation in the inferior vena cava of mice. Platelets. 2013; 24:205–212. [PubMed: 22720736]
24. Methia N, Andre P, Denis CV, Economopoulos M, Wagner DD. Localized reduction of atherosclerosis in von Willebrand factor-deficient mice. Blood. 2001; 98:1424–1428. [PubMed: 11520791]
25. Massberg S, Brand K, Gruner S, Page S, Muller E, Muller I, Bergmeier W, Richter T, Lorenz M, Konrad I, Nieswandt B, Gawaz M, Schurzinger K, Lorenz M, Konrad I, Schulz C, Plesnila N, Kennerknecht E, Rudelius M, Sauer S, Braun S, Kremmer E, Emambokus NR, Frampton J, Gawaz M, Langer H, May AE. A critical role of platelet adhesion in the initiation of atherosclerotic lesion formation. J Exp. Med. 2002; 196:887–896. [PubMed: 12370251]
26. Theilmeier G, Michiels C, Spaepen E, Vreys I, Collen D, Vermylen J, Hoylaerts MF. Endothelial von Willebrand factor recruits platelets to atherosclerosis-prone sites in response to hypercholesterolemia. Blood. 2002; 99:4486–4493. [PubMed: 12036879]
27. Wu H, Gower RM, Wang H, Perrard XY, Ma R, Bullard DC, Burns AR, Paul A, Smith CW, Simon SI, Ballantyne CM. Functional role of CD11c+ monocytes in atherogenesis associated with hypercholesterolemia. Circulation. 2009; 119:2708–2717. [PubMed: 19433759]
28. Furman MI, Benoit SE, Barnard MR, Valeri CR, Borbone ML, Becker RC, Hechtman HB, Michelson AD. Increased platelet reactivity and circulating monocyte-platelet aggregates in patients with stable coronary artery disease. J. Am. Coll. Cardiol. 1998; 31:352–358. [PubMed: 9462579]
29. Furman MI, Barnard MR, Krueger LA, Fox ML, Shilale EA, Lessard DM, Marchese P, Frelinger AL III, Goldberg RJ, Michelson AD. Circulating monocyte-platelet aggregates are an early marker of acute myocardial infarction. J. Am. Coll. Cardiol. 2001; 38:1002–1006. [PubMed: 11583872]

30. Sarma J, Laan CA, Alam S, Jha A, Fox KA, Dransfield I. Increased platelet binding to circulating monocytes in acute coronary syndromes. Circulation. 2002; 105:2166–2171. [PubMed: 11994250]
31. Keating FK, Whitaker DA, Kabbani SS, Ricci MA, Sobel BE, Schneider DJ. Relation of augmented platelet reactivity to the magnitude of distribution of atherosclerosis. Am. J. Cardiol. 2004; 94:725–728. [PubMed: 15374774]
32. Huo Y, Schober A, Forlow SB, Smith DF, Hyman MC, Jung S, Littman DR, Weber C, Ley K. Circulating activated platelets exacerbate atherosclerosis in mice deficient in apolipoprotein E. Nat. Med. 2003; 9:61–67. [PubMed: 12483207]
33. Wu H, Perrard XD, Wang Q, Perrard JL, Polsani VR, Jones PH, Smith CW, Ballantyne CM. CD11c expression in adipose tissue and blood and its role in diet-induced obesity. Arterioscler. Thromb. Vasc. Biol. 2010; 30:186–192. [PubMed: 19910635]
34. Xu L, Dai X P, Perrard JL, Yang D, Xiao X, Teng BB, Simon SI, Ballantyne CM, Wu H. Foamy monocytes form early and contribute to nascent atherosclerosis in mice with hypercholesterolemia. Arterioscler. Thromb. Vasc. Biol. 2015; 35:1787–1797. [PubMed: 26112011]
35. Foster GA, Xu L, Chidambaram AA, Soderberg SR, Armstrong EJ, Wu H, Simon SI. CD11c/CD18 Signals Very Late Antigen-4 Activation To Initiate Foamy Monocyte Recruitment during the Onset of Hypercholesterolemia. J. Immunol. 2015; 195:5380–5392. [PubMed: 26519532]
36. Savage B, Saldivar E, Ruggeri ZM. Initiation of platelet adhesion by arrest onto fibrinogen or translocation on von Willebrand factor. Cell. 1996; 84:289–297. [PubMed: 8565074]
37. Savage B, Almus-Jacobs F, Ruggeri ZM. Specific synergy of multiple substrate-receptor interactions in platelet thrombus formation under flow. Cell. 1998; 94:657–666. [PubMed: 9741630]
38. Kroll MH, Harris TS, Moake JL, Handin RI, Schafer AI. von Willebrand factor binding to platelet GpIb initiates signals for platelet activation. J. Clin. Invest. 1991; 88:1568–1573. [PubMed: 1939645]
39. Savage B, Shattil SJ, Ruggeri ZM. Modulation of platelet function through adhesion receptors. A dual role for glycoprotein IIb-IIIa (integrin αIIb β3) mediated by fibrinogen and glycoprotein Ib-von Willebrand factor. J. Biol. Chem. 1992; 267:11300–11306. [PubMed: 1597464]
40. Cruz MA, Chen J, Whitelock JL, Morales LD, Lopez JA. The platelet glycoprotein Ib-von Willebrand factor interaction activates the collagen receptor alpha2beta1 to bind collagen: activation-dependent conformational change of the alpha2-I domain. Blood. 2005; 105:1986–1991. [PubMed: 15514009]
41. Xu G, Shang D, zhang Z, Shaw TS, Ran Y, Lopez JA, Peng Y. The transmembrane domains (TMDs) of ß and IX subunits mediate the localization of the platelet glycoprotein Ib-IX complex to the glycosphingolipid-enriched membrane domain. J. Biol. Chem. 2015 In press.
42. Koltsova EK, Sundd P, Zarpellon A, Ouyang H, Mikulski Z, Zampolli A, Ruggeri ZM, Ley K. Genetic deletion of platelet glycoprotein Ib alpha but not its extracellular domain protects from atherosclerosis. Thromb. Haemost. 2014; 112:1252–1263. [PubMed: 25104056]

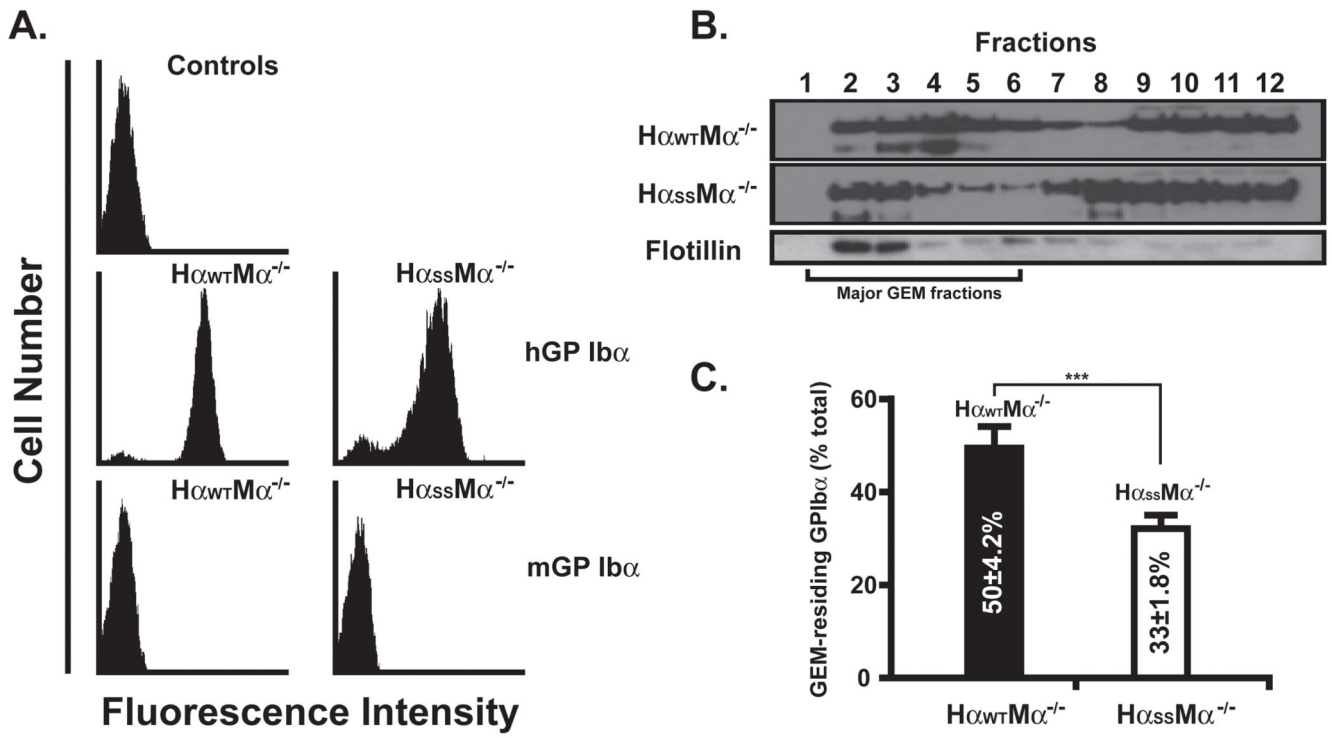

FIGURE1.

Disruption of α/β disulfide linkage inhibits the association of transgenic GP Ibα with the murine platelet GEMs. ***A.*** Murine whole blood was incubated with either a PE-labeled mouse anti-human GP Ibα or a FITC-labeled rat anti-mouse GP Ibα monoclonal antibody. ***B.*** The GP Ibα GEMs associations were revealed by sucrose gradient density fractionation and western blotting (n=8). The GEMs fractions are identified by the presence of flotillin, a known GEM-specific marker. ***C.*** The GEMs association level of GP Ibα is presented as the percentage of GEMs-associating GP Ibα in respect to the total GP Ibα across all sucrose density fractions. All experiments and measurements were done at least 3 times.

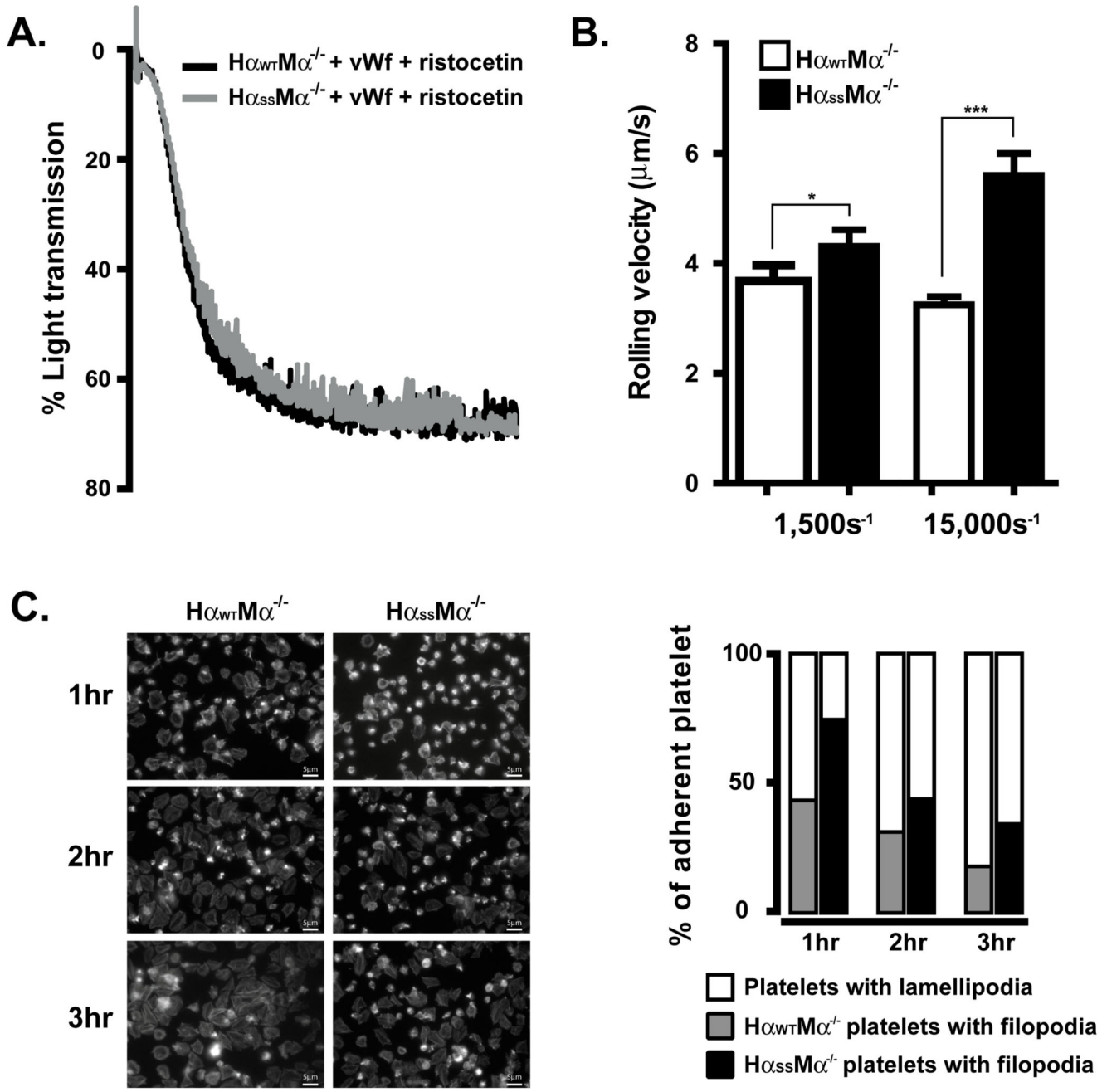

FIGURE 2.

Transgenic GP Ib-IX function is impaired due to a GEMs-association dysfunction. ***A.*** The aggregometry analyses of vWf binding to transgenic platelets (2×10^5/μl) were performed in the presence of 1.5mg/ml ristocetin. ***B.*** The murine whole blood was perfused over a human vWf-coated surface in a parallel-plate flow chamber at shear rates of either $1{,}500s^{-1}$ or $15{,}000s^{-1}$. ***C.*** The rhodamine-conjugated phalloidin staining showed that transgenic platelets changed their morphology from filopodia protrusion to lamellipodia upon binding to immobilized vWf. Each experiment was performed at least 3 times and the error bars in

rolling experiments were calculated from the mean rolling velocities of at least 100 cells in 5 different view fields.

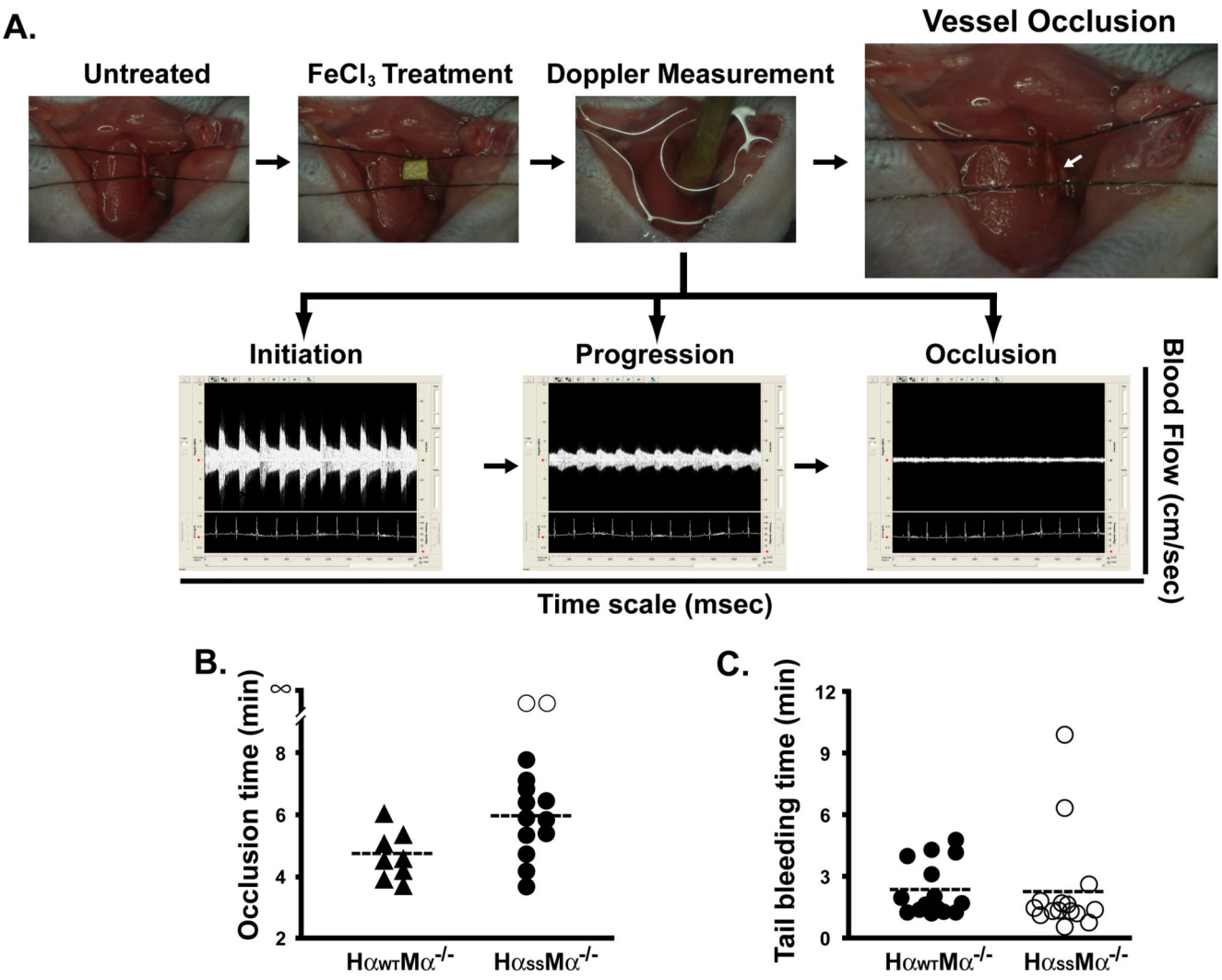

FIGURE 3.

Dysfunction in the GP Ib-IX-GEMs association delays the formation of a $FeCl_3$-induced thrombus in the carotid artery. ***A.*** Murine right common carotid artery was exposed to a 10×10 mm strip of 3MM Waterman filter paper saturated in a 10% $FeCl_3$ solution (upper panel). The blood flow and ECG signals were monitored using a PC-based high-speed real-time Doppler signal processing system (lower panel). The occlusion time was counted as the period from the removal of the filter paper to the time when the Doppler signal went to nearly zero. ***B***. The average occlusion time for the wild-type mice ($H\alpha_{WT}$, n=8) was approximately ~1min shorter than that for the mutant animals ($H\alpha_{SS}$, n=14). C. Mouse tail bleeding time was defined as the time from incision to cessation of blood.

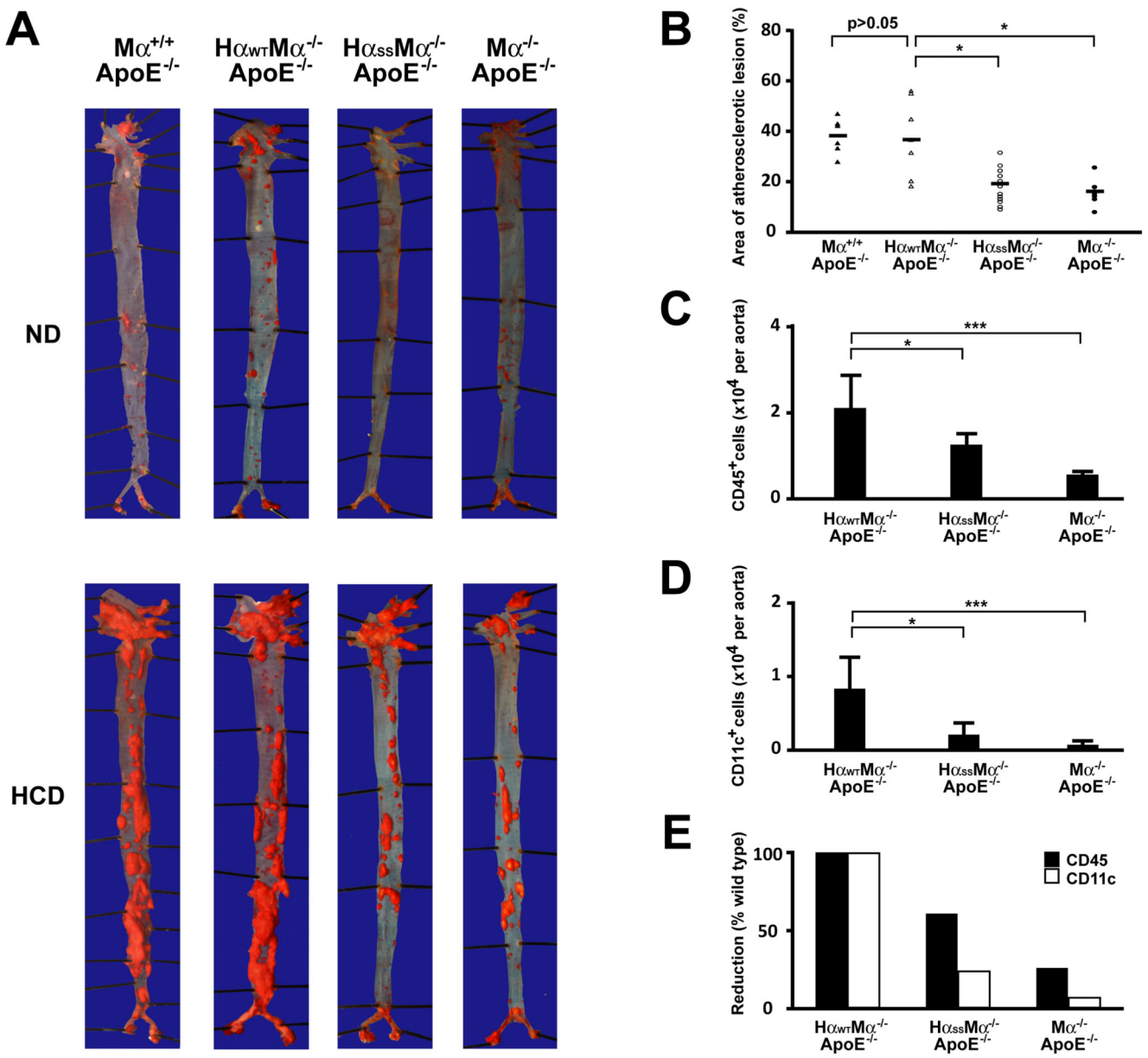

FIGURE 4.

GEMs association dysfunctional GP Ibα mitigates atheroma formation in ApoE deficient animals fed HCD. All samples were collected from mice on HCD for 16 weeks starting at the age of 6 months. ***A.*** Representative oil red staining of the aortas of mice (n=12) fed either HCD or normal diet (ND). ***B.*** Quantification of atherosclerotic lesions in whole aortas was done using Image J software. Mouse aortas were digested with a mixture of enzymes and the $CD45^+$ (***C***) and $CD11c^+$ (***D***) leukocytes were counted in aortas of 16 weeks HCD-fed animals (n=8 of each group, age and gender matched). ***E.*** The $CD11c^+$ cells are reduced to a greater extent than other $CD45^+$ cell types in mutant and GP Ibα deficient mice when compared to the wild type animals.

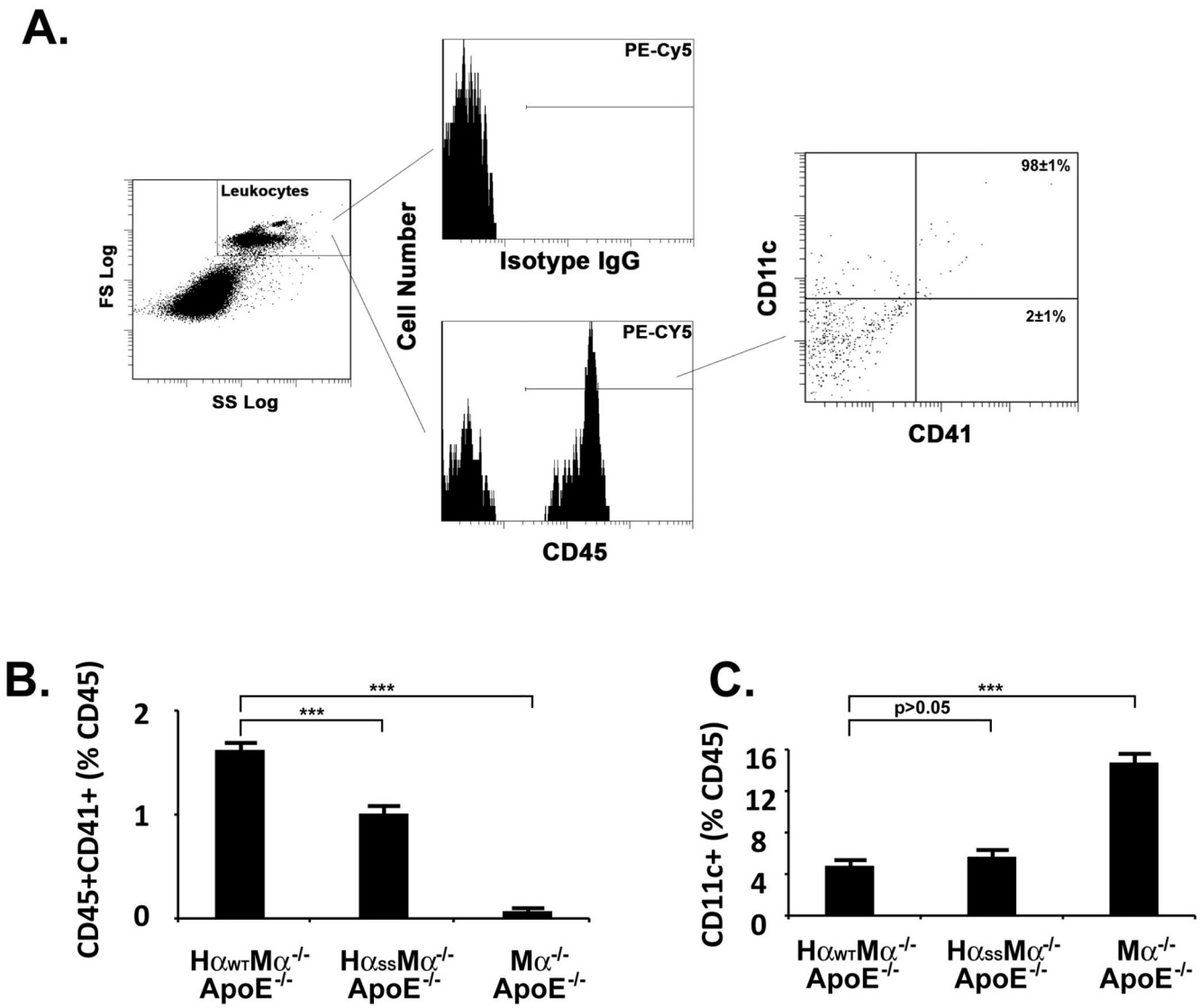

FIGURE 5.

CD11c^{+} leukocytes are the dominant cell type in circulation that can aggregate with platelets in atherosclerotic mice. (***A***) PE-Cy5-labeled anti-mouse CD45 antibody was used to gate the leukocyte population in whole blood samples pooled from atherosclerotic mice (n=12 of each group, age and gender matched). The percentages of the CD45 cells in complex with the platelet (CD41, ***B***) or co-expressing CD11c antigen (***C***) were measured by flow cytometry. All experiments and measurements were done at least 3 times and the error bars were calculated from the mean % values acquired from all experiments performed.

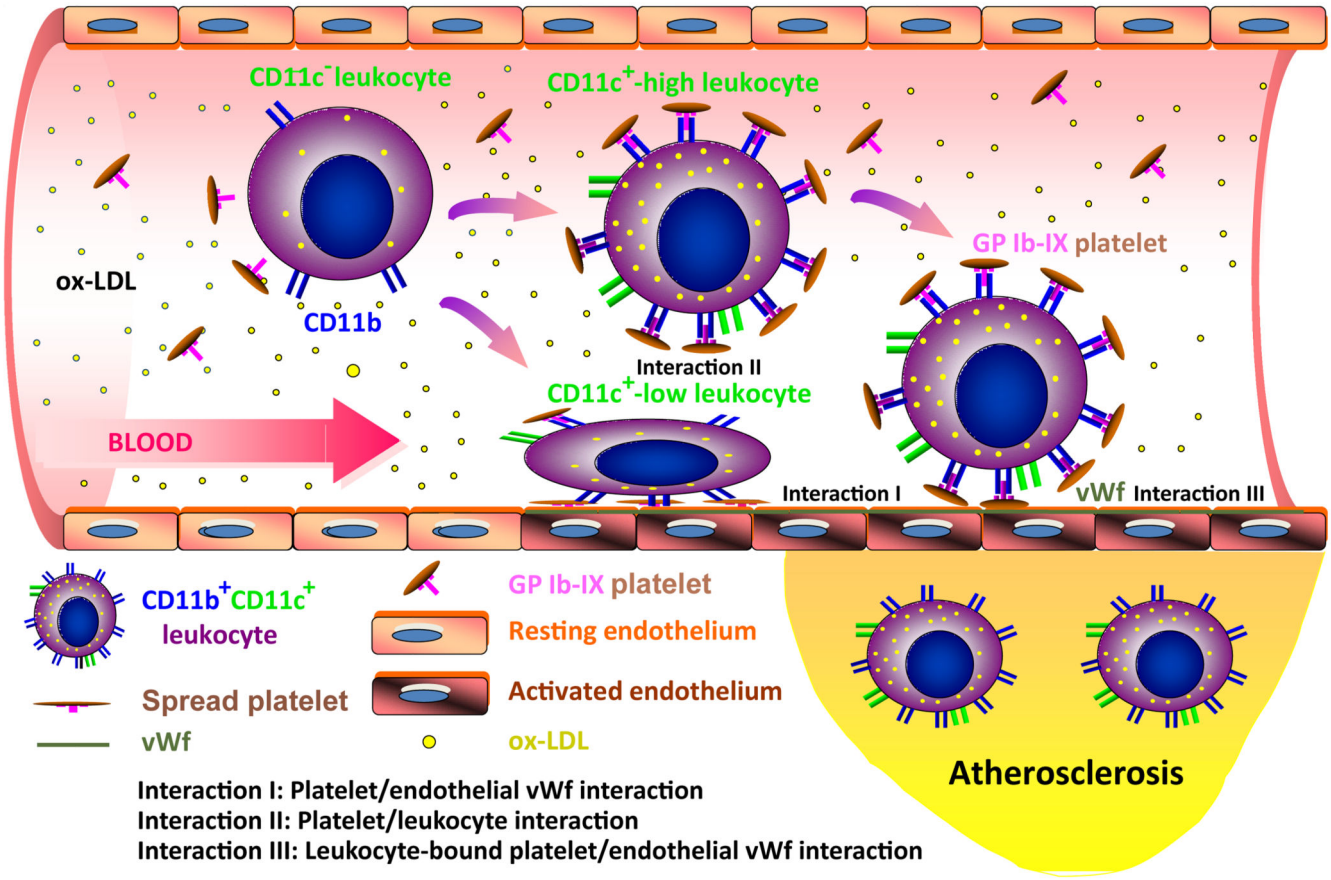

FIGURE 6.

A hypothesized model for the platelet-mediated recruitment and infiltration of $CD11c^+$ leukocytes to atherosclerotic vessel walls. Upon uptake of oxidized low-density lipoprotein (ox-LDL), the circulating leukocytes differentiate from a $CD11c^-$ to a $CD11c^+$ phenotype and increase the expression of activated CD11b (or other GP Ib-IX complex ligands) on their surfaces. In circulation, these $CD11c^+CD11b^+$ leukocytes may be captured by platelets that are anchored by endothelial vWf (Interaction I), or pre-bound with flowing platelets (Interaction II) and then recruited by endothelial vWf (Interaction III) in a shear-dependent manner. Dysfunction in the GEM association may inhibit these GP Ib-IX complex-mediated interactions, which causes inefficient recruitment and infiltration of the $CD11c^+$ leukocytes to the atherosclerotic vessel wall. Of note, This illustration is revised from an image published previously (27).